

# HIGH-RESOLUTION DIRECTION-OF-ARRIVAL ESTIMATION IN SNR AND SNAPSHOT CHALLENGED SCENARIOS USING MULTI-FREQUENCY COPRIME ARRAYS

Yang Liu John R. Buck\*

{yang.liu, j buck}@umassd.edu  
Electrical and Computer Engineering Department  
University of Massachusetts Dartmouth

## ABSTRACT

This paper proposes two high-resolution Direction-of-Arrival (DOA) estimators using coprime sensor arrays (CSA) processing broadband signals. The product processor estimates the broadband spatial power spectral density (PSD) by averaging narrowband spatial PSD estimates. These narrowband PSD estimates are formed by multiplying one CSA subarray scanned response with the complex conjugate of the other. Contrastingly, the min processor estimates the broadband spatial PSD by taking the minimum over all subarray periodograms at all processed frequencies for each bearing. The inverse Fourier transform of the broadband spatial PSD estimates the spatial correlation function, which populates the diagonals of a Toeplitz augmented covariance matrix (ACM). The MUSIC algorithm estimates the source DOAs from this constructed ACM. Combining the CSA narrowband PSD estimates over additional bandwidth reduces the number of snapshots needed to attenuate cross-terms in the spatial PSD estimates, providing processing gains for DOA estimation. The MUSIC pseudo-spectra suggest that the product algorithm performs better in scenarios with more sources than sensors and the min algorithm performs better in scenarios with varying source power levels. Monte Carlo simulations show that the new DOA estimators achieve improved precision over previous broadband CSA DOA estimators in snapshot-challenged scenarios.

**Index Terms**— Coprime arrays, multi-frequency, product processing, min processing, DOA estimation

## 1. INTRODUCTION

Direction-of-Arrival (DOA) estimation is a major application of coprime sensor arrays (CSA) in radar, sonar and communication systems [1, 2, 3, 4]. There are in general two approaches to process the CSA data. The first approach directly estimates the second-order statistics of the propagating field from the array data and is termed spatial correlation processing in this paper. For a CSA with  $O(N)$  sensors, applying spatial smoothing MUSIC on the correlation estimates is able to identify up to  $O(N^2)$  closely-spaced uncorrelated sources given sufficient data snapshots [5]. Alternatively, a product processor applies conventional beamforming (CBF) separately on the CSA subarray data and then multiplies one subarray scanned response with the complex conjugate of the other [1]. This CSA product processor resolves the aliasing in the spatial power spectral density (PSD) estimates and achieves the resolution of the fully populated ULA spanning a comparable aperture [4].

Spatial correlation processing and product processing are implicitly related. The correlation processing estimates the spatial cor-

relation lags from pairs of sensors with appropriate spacings, which is equivalent to cross-correlating the ‘zero-filled’ subarrays data followed by appropriate windowing and normalization [6]. The correlation processing algorithm is an extension of Pillai *et al.*’s augmented covariance matrix (ACM) DOA estimation algorithm [7, 8] to include two co-linear subarrays, as opposed to one single minimum redundancy array. Subarray cross-correlation in the spatial domain is equivalent to multiplying one subarray scanned response with the complex conjugate of the other in the spatial frequency domain. Therefore, the statistical properties of the product spectrum implicitly impact the high-resolution DOA estimators using the ACM constructed from the co-array correlation estimates. Issues created by the non-positive semi-definite spectrum occur with pairwise correlation estimates before any of the spatial smoothing steps as proposed in [2, 5]. As a result, the ACM constructed from the co-array correlation estimates is not guaranteed positive semi-definite [7, 8]. The variance of the CSA product periodogram is higher than the variance of the fully populated ULA periodogram spanning a comparable aperture [6]. This explains the reduced precision in the DOA estimates for multiple sources using the correlations estimated from the CSA rather than the fully populated ULA [3, 5]. The CSA product periodogram requires a large number of snapshots to statistically average out the cross-terms in presence of multiple sources [1, 4, 9]. Consequently, many proposed high-resolution DOA estimators using nested arrays and CSAs either explore the ensemble behavior or focus on asymptotic performance for relatively high SNR and large numbers of snapshots [1, 2, 3, 5, 10, 11]. These assumptions ensure less biased and more precise estimates of the second-order statistics of the propagating field from the array data. However, both the noise level and the number of snapshots assumed in those papers are unrealistically optimistic for many acoustic environments, largely due to the speed of acoustical field propagation, use of large array apertures and the field being non-stationary [12, 13].

We propose new broadband CSA processing algorithms that detect and estimate the DOAs of more sources than sensors with improved precision in low SNR and snapshot-challenged scenarios. The proposed algorithms exploit the duality between CSA narrowband beamforming and undersampled ULA broadband beamforming in spatial PSD estimation. The CSA narrowband beamformer exploits the beam responses obtained through the spatial sampling diversity across multiple subarrays to attenuate grating lobes while processing a single narrowband frequency. The ULA broadband beamformer exploits the beam responses obtained through the frequency diversity across the signal bandwidth to attenuate grating lobes while processing a single spatially undersampled array [14]. Combining both sampling and frequency diversity results in processing gains for high-resolution DOA estimation over the performance

\*Supported by the ONR BRC Program grant N00014-13-1-0230.

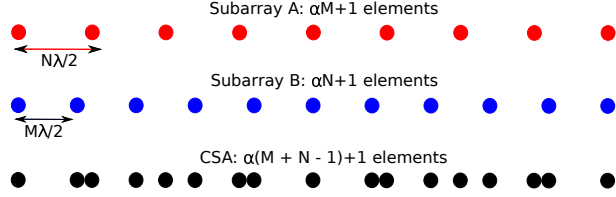


**Fig. 1.** Extended center-symmetric coprime sensor array geometry for  $(M, N) = (4, 5)$  and extension factor  $\alpha = 2$ . The CSA interleaves two subarrays A and B, which have the same aperture and share  $\alpha + 1$  sensors. CSA has  $\alpha(M + N - 1) + 1$  sensors in total.

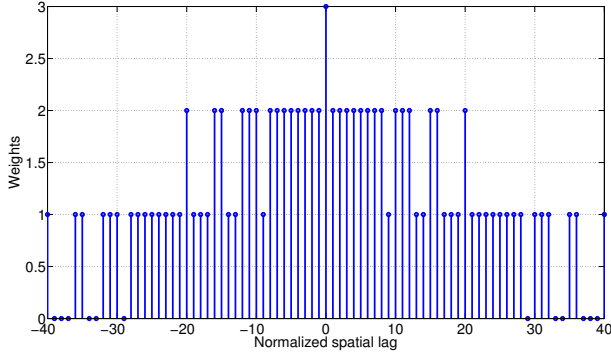


**Fig. 2.** Cross-correlation difference co-array weights of the CSA geometry in Fig. 1 with  $(M, N) = (4, 5)$  and  $\alpha = 2$ . The co-array spans  $k \in [-40, 40]$ , with missing lags (holes) occurring at  $\pm 29, \pm 33, \pm 34, \pm 37, \pm 38, \pm 39$ .

achieved by either beamformer acting alone.

This paper assumes that the underlying propagating field is stochastically wide-sense stationary, the sources are uncorrelated, and the signal observation time is long enough that the data snapshots at distinct frequencies are uncorrelated. Although both algorithms assume relatively broadband signals, the proposed DOA estimators differ from the broadband CSA DOA estimator proposed in [3] in two ways. First, Ref. [3] assumes the source spectra at different frequencies are proportional, and violating this requirement leads to larger DOA estimation errors using the algorithm in [15]. In contrast, the source spectra in this paper are not assumed to be proportional, but only assumed to occupy sufficiently wide frequency bandwidth (typically within  $\pm 10\%$  around the nominal frequency) with meaningful power at each frequency. Second, Ref. [3] enlists the array data for a small set of sensor pairs at a set of additional temporal frequencies to estimate the spatial correlations at the missing co-array lags (holes) to construct a larger covariance matrix for localizing more sources. In contrast, this paper processes the data at these same frequencies to estimate a full spatial PSD, thus implicitly estimating the correlation function for all lags at all processed frequencies, not just a small subset.

## 2. COPRIME SENSOR ARRAYS AND CO-ARRAYS

A CSA interleaves two spatially undersampled ULAs, referred to as subarrays, with coprime undersampling factors  $M$  and  $N$  sharing no common divisor greater than 1 (Fig. 1). In this paper, the coprime factors satisfy  $N = M + 1$ , which minimizes the sensors required to span a given array aperture [4]. Subarray A has  $\alpha M + 1$  sensors

with intersensor spacing  $N\lambda/2$  and subarray B has  $\alpha N + 1$  sensors with intersensor spacing  $M\lambda/2$ , where  $\lambda$  is the wavelength of the incoming plane wave at the nominal frequency  $f_0$ . The array aperture extension factor  $\alpha$  is assumed an integer for simplicity. The two subarrays are aligned at both ends and center symmetric and therefore share  $\alpha + 1$  sensors. As a result, the CSA has  $\alpha(M + N - 1) + 1$  total sensors spanning an aperture of  $\alpha MN\lambda/2$ . High-resolution line spectral estimation makes use of the second-order statistics of the underlying field such as acoustic or electromagnetic waves. Spatial correlation processing the sparse arrays data offers more than twice the number of degrees-of-freedom (DOFs), or distinct difference co-array lags, as the physical sensors, and thereby can localize more sources than sensors [5, 7, 8]. Fig. 2 shows the cross-correlation difference co-array weights for the CSA geometry in Fig. 1. The weight value indicates the number of sensor pairs corresponding to the same co-array lag. The co-array spans lags from  $\pm\alpha M(M + 1)$ , with its weights symmetric about the co-array center. There are  $M(M - 1)$  missing correlation lags (holes) in the full co-array span and the hole-free region spans  $\pm((\alpha - 1)M(M + 1) + 2M)$ .

## 3. DOA ESTIMATION USING MULTI-FREQUENCY CSA PRODUCT AND MIN PROCESSORS

Combining the CSA narrowband PSD estimates over additional bandwidth reduces the number of snapshots needed to attenuate the cross-terms in the spatial PSD estimates, providing processing gains for high-resolution DOA estimation. This paper uses directional cosine  $u = \cos(\theta)$  to indicate the source directions, where  $\theta \in [0^\circ, 180^\circ]$  is the DOA with respect to the array axis. Fig. 3 illustrates the proposed data processing procedures using the  $\text{CSA}_{\text{product}}$  or  $\text{CSA}_{\text{min}}$  processors when the sources are broadband in temporal frequency. The DOA estimators contain two major steps: broadband spatial PSD estimation (Figs. 3a-b) and Toeplitz ACM construction for spectral MUSIC (Fig. 3c). The two broadband spatial PSD estimators in step 1 differ in the way they combine the narrowband spatial PSD estimates by averaging across frequencies (Fig. 3a) or using the min processor (Fig. 3b). At each temporal frequency  $f_l, l = 1, \dots, L$  for narrowband spatial PSD estimation, the CSA subarrays are separately conventionally beamformed to produce two spatial scanned responses  $y_{a,l}(u)$  and  $y_{b,l}(u)$  for the narrowband snapshot data corresponding to  $f_l$ . Each subarray scanned response contains grating lobes due to the spatial undersampling. For a single source, multiplying one subarray output with the complex conjugate of the other at each bearing resolves the aliasing ambiguities. In the presence of multiple sources, the cross-power spectra have multiple cross-terms, which typically require averaging large number of snapshots to be attenuated [1, 4, 9]. However, in broadband processing, only the true source DOA peaks are fixed across frequencies, while the cross-terms change locations in  $u$  as the frequency changes. As a result of averaging across frequencies [14]

$$t_{cp}(u) = \frac{1}{L} \sum_{l=1}^L |y_{a,l}(u)y_{b,l}^*(u)|, \quad (1)$$

the peaks at the true source DOAs are constructively reinforced, while the cross-terms are relatively attenuated.

Liu and Buck [16] proposed the min processor to guarantee a positive semi-definite spatial PSD estimate for the narrowband CSA data. At each temporal frequency, the min processor chooses the minimum between the two subarray periodograms at each bearing to resolve the subarray aliasing ambiguities (Fig. 3b). The min processor mitigates the destructive interference of weaker sources by

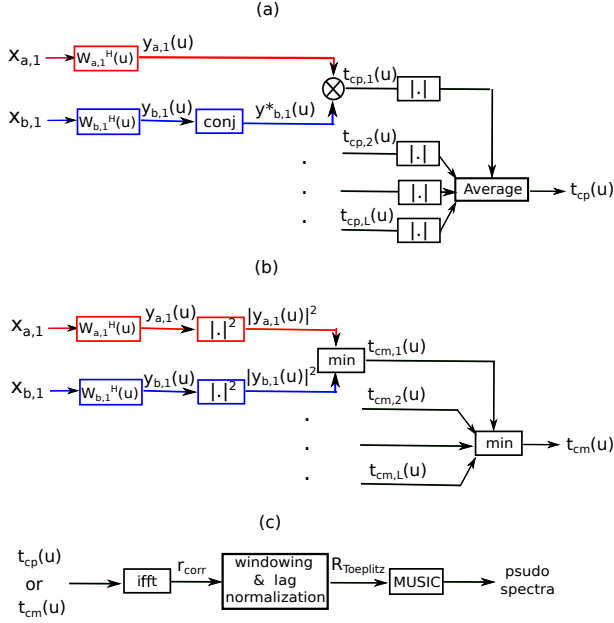


**Fig. 3.** Block diagrams for broadband coprime array PSD estimates using the product processor (a) and min processor (b). The broadband spatial PSD estimates from either  $\text{CSA}_{\text{product}}$  or  $\text{CSA}_{\text{min}}$  are used for high-resolution DOA estimation using spectral MUSIC (c).

the negative sidelobes of strong sources in the CSA product spectra. In the presence of multiple sources, the min spectra may also have cross-terms, which will persist with snapshot averaging. Again, in broadband processing, the true source DOA peaks are fixed across frequencies while the cross-terms change locations in  $u$  as the frequency changes. Taking the minimum of the spatial spectra estimated across all frequencies at each bearing

$$t_{cm}(u) = \min_l \left( \min_{a,b} (|y_{a,l}(u)|^2, |y_{b,l}(u)|^2) \right), \quad (2)$$

the peaks at the true source DOAs are well preserved, while the cross-terms are relatively attenuated.

Given the broadband spatial PSD estimates, the second step of the DOA estimators involves the ACM construction and spectral MUSIC. The inverse Fourier transform of the PSD estimates from the product processor  $t_{cp}(u)$  or the min processor  $t_{cm}(u)$  provides estimates of the spatial correlation function  $\hat{r}_{corr}(k)$ . We apply windowing to  $\hat{r}_{corr}(k)$  to extract the region corresponding to the span of the difference co-array. The estimated correlation function  $\hat{r}_{corr}(k)$  is then normalized by the corresponding co-array weights to correct for the bias due to redundancies at certain lags. The correlation estimates at the missing co-array lag positions are implicitly interpolated by the inverse Fourier transform. This approach allows us to exploit all the DOFs in the co-array span. The normalized correlation estimates populate the diagonals of a Hermitian Toeplitz ACM. The MUSIC algorithm then processes the constructed ACM to separate the signal and noise subspaces for high-resolution pseudo-spectra estimation [10, 17].

#### 4. SIMULATION RESULTS

To compare the performance of the proposed multiple frequency DOA estimation algorithms, we consider the CSA configuration in

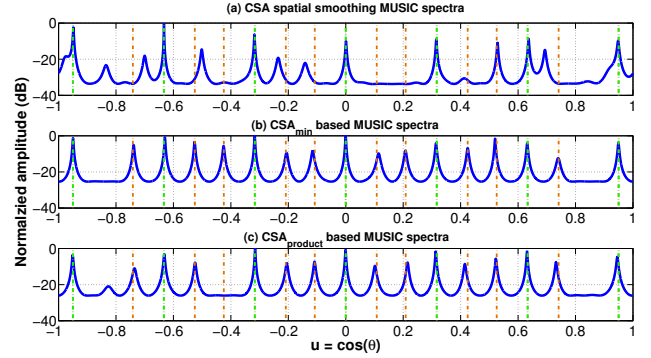


**Fig. 4.** Comparison of three multi-frequency algorithms' MUSIC pseudo-spectra on a dB scale against directional cosine  $u = \cos \theta$  for multiple incoming sources of different powers: strong sources with sensor level SNR = 0 dB are indicated by green lines and weak sources with SNR = -10 dB are indicated by orange lines. The CSA has 17 sensors in total and all simulations use 17 independent data snapshots.

Fig. 1 with  $(M, N) = (4, 5)$  and  $\alpha = 2$ . Subarray A consists of 9 sensors located at indices  $\{1, 6, 11, 16, 21, 26, 31, 36, 41\}$  and subarray B consists of 11 sensors located at indices  $\{1, 5, 9, 13, 17, 21, 25, 29, 33, 37, 41\}$ . The two subarrays share 3 sensors at locations  $\{1, 21, 41\}$  and therefore the CSA has 17 sensors in total. The difference co-array spans  $k \in [-40, 40]$ , among which the 57 lags within  $k \in [-28, 28]$  are contiguous. There are 12 missing lags occurring at  $k = \pm 29, \pm 33, \pm 34, \pm 37, \pm 38, \pm 39$ . All simulation results presented below assume *a priori* knowledge of the correct number of sources, consistent with previous literature on DOA estimation with sparse arrays [1, 2, 3, 5, 10, 11].

Single frequency MUSIC based on either a spatially smoothed covariance matrix [2, 5] or Toeplitz covariance matrix augmentation [8, 10] can only use the contiguous portion of the co-array estimates. Therefore, up to 28 uncorrelated sources can be localized provided sufficient snapshots and relatively high SNR are available. For the CSA geometry in Fig. 1, the multi-frequency algorithm in [3] requires 6 additional frequencies to estimate the missing co-array lags. Specifically, the additional frequencies and sensor pairs employed are  $f_1 = (29/30)f_0$  and sensor pair  $\{1, 31\}$  to fill in co-array hole  $k = \pm 29$ ,  $f_2 = (33/35)f_0$  and  $\{1, 36\}$  to fill in  $k = \pm 33$ ,  $f_3 = (34/35)f_0$  and  $\{1, 36\}$  to fill in  $k = \pm 34$ ,  $f_4 = (37/40)f_0$  and  $\{1, 41\}$  to fill in  $k = \pm 37$ ,  $f_5 = (38/40)f_0$  and  $\{1, 41\}$  to fill in  $k = \pm 38$  and  $f_6 = (39/40)f_0$  and  $\{1, 41\}$  to fill in  $k = \pm 39$ . All of the additional frequencies fall within 8% of the nominal frequency  $f_0$ . With all co-array holes filled, spatially smoothed MUSIC is able to localize up to 40 uncorrelated sources. To make a fair comparison with the multi-frequency CSA MUSIC algorithm in [3], the multi-frequency  $\text{CSA}_{\text{product}}$  and  $\text{CSA}_{\text{min}}$  based algorithms proposed in this paper use exactly the same frequencies and range of co-array lags within  $k \in [-40, 40]$  for high resolution DOA estimation.

The simulations compare the performance of three different broadband DOA estimators: the hole-filling spatially smoothed algorithm in [3], the proposed  $\text{CSA}_{\text{product}}$  based algorithm in Fig. 3(a) and the  $\text{CSA}_{\text{min}}$  based algorithm in Fig. 3(b). The first scenario simulates the performance of the DOA estimators for multiple sources with varying power levels. The sources' DOAs are designed with 7 strong sources (0 dB sensor SNR, green lines) uniformly spaced

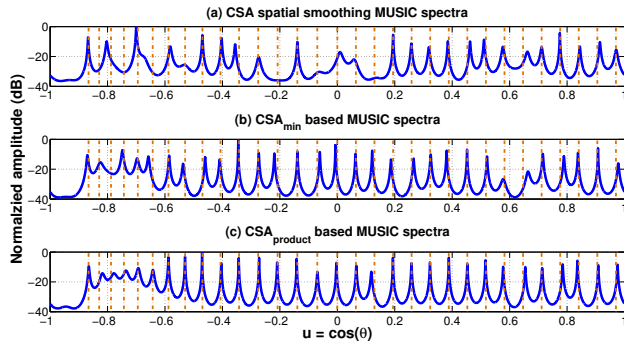


**Fig. 5.** Comparison of three multi-frequency algorithms' MUSIC pseudo-spectra on a dB scale for a scenario with more sources than number of sensors. There are 31 uncorrelated sources arrives at the array: 1 at broadside, 15 uniformly spaced in  $u \in (0, 0.97]$  and another 15 uniformly spaced in  $\theta \in (90^\circ, 150^\circ]$ . The sensor level SNR for all sources is 0 dB. The CSA has 17 sensors in total and all simulations use 34 independent data snapshots.

in  $u \in [-0.95, 0.95]$ , interleaved with two weaker sources for each strong source (-10 dB SNR, orange lines) offset in DOA by  $\Delta u = \pm 0.42$ , the negative peak sidelobe locations at the nominal frequency. The 4 weaker source locations that fall outside the visible range are not included, resulting in a total of 17 sources for the 17 element CSA. Fig. 4 compares the MUSIC pseudo-spectra for this scenario with 17 independent data snapshots at each frequency. Fig. 4(a) shows the spatial smoothing algorithm fails to detect all weak sources and exhibits biases for certain DOAs. Fig. 4(b) shows the  $CSA_{\min}$  algorithm localizes all sources successfully even in this SNR and snapshot-challenged scenario since its spatial spectra is guaranteed positive semi-definite. Fig. 4(c) shows the  $CSA_{\text{product}}$  algorithm detects most sources correctly, but misses detecting the peak at  $u = -0.42$  because the negative sidelobes of the strong source at broadside destructively mask the weak source for the product spectra.

The second scenario compares the DOA estimators for the case with more sources than sensors. There are 31 uncorrelated sources in presence with the same sensor SNR of 0 dB: 1 at broadside, 15 uniformly spaced in  $u \in (0, 0.97]$  and another 15 uniformly spaced in  $\theta \in (90^\circ, 150^\circ]$ . Fig. 5 compares the MUSIC pseudo-spectra for the three DOA estimators with 34 independent data snapshots at each frequency. The orange dashed lines in all panels indicate the true source DOAs. Fig. 5(a) shows the spatial smoothing algorithm fails to detect multiple sources due to lack of snapshots. Fig. 5(b) shows the  $CSA_{\min}$  algorithm correctly locates most sources, but misses detecting the peak at  $u = -0.79$ . Fig. 5(c) shows the  $CSA_{\text{product}}$  algorithm successfully locates all incoming sources, although the 6 left-most peaks are less distinguishable than others.

To compare the performance of different DOA estimators in snapshot challenged scenarios, we evaluate the average root mean square error (RMSE) of all estimated DOAs against the number of snapshots per sensor. The error is calculated as  $RMSE = (\sum_{d=1}^D \sum_{q=1}^Q (\hat{\theta}_d(q) - \theta_d)^2 / DQ)^{1/2}$ , where  $\hat{\theta}_d(q)$  is the estimated angle of arrival for the  $d$ -th source in the  $q$ -th Monte Carlo trial,  $D$  is the number of sources and  $Q$  is the number of Monte Carlo trials. Fig. 6 compares the RMSEs averaged over 500 Monte Carlo trials of the six algorithms for the same scenario as in Fig. 5.

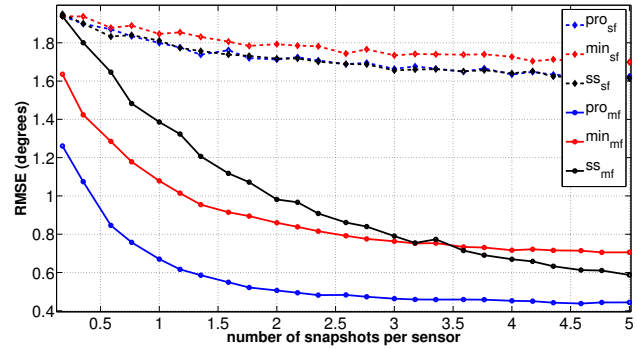


**Fig. 6.** Comparing the RMSE for the estimated angles of arrival of six algorithms against number of snapshots per sensor averaged over 500 Monte Carlo trials. 'sf' and 'mf' indicates single and multiple frequency algorithms respectively. Sensor level SNR is 0 dB for all sources. The 31 sources are distributed as in Fig. 5.

Note how the RMSEs converge for all algorithms as the number of snapshots per sensor increases. Specifically, the RMSEs for all single frequency algorithms operating at the nominal frequency  $f_0$  decrease slowly and are all above 1.6 degrees. This is expected since single frequency CSA MUSIC is able to localize at most 28 sources in this case and therefore struggles to estimate all source DOAs. On the other hand, applying multiple frequencies expands the applicable DOFs in the co-array, allowing estimation of more source DOAs. The RMSEs of all three multi-frequency algorithms are lower than their single frequency counterparts and also converge faster as the number of snapshots per sensor increases. The proposed multi-frequency  $CSA_{\min}$  has lower RMSE than the multi-frequency spatial smoothing algorithm for less than 3 snapshots per sensor. The multi-frequency  $CSA_{\text{product}}$  has much lower RMSE than the multi-frequency spatial smoothing algorithm over the entire range examined.

## 5. CONCLUSION

This paper proposes two high-resolution source DOA estimators by applying the product and min processors on multi-frequency coprime sensor arrays. The spatial correlations implied from the PSD estimates populate the diagonals of a Hermitian Toeplitz augmented covariance matrix. Applying high resolution spectral MUSIC to the constructed ACM localizes more spatially uncorrelated narrow-band sources than the number of sensors. Simulations show that the proposed multi-frequency algorithms improve high-resolution DOA estimation for CSAs in low SNR and snapshot-challenged scenarios. The multi-frequency  $CSA_{\text{product}}$  DOA estimator improves the estimation performances for more sources than sensors in snapshot-challenged scenarios. The multi-frequency  $CSA_{\min}$  DOA estimator is able to identify relatively weak sources located in the negative sidelobes of the strong sources since the PSD estimates are guaranteed positive semi-definite. Adding bandwidth for averaging greatly reduces the amount of snapshots needed to reduce the cross-terms in the product spectra estimates. A future research focus is a more rigorous characterization of these improved DOA estimation performance in less restrictive scenarios for both source powers and DOAs.

## 6. REFERENCES

- [1] P.P. Vaidyanathan and P. Pal, "Sparse sensing with co-prime samplers and arrays," *IEEE Trans. Signal Process.*, vol. 59, no. 2, pp. 573-586, 2011.
- [2] P. Pal and P.P. Vaidyanathan, "Nested arrays: a novel approach to array processing with enhanced degrees of freedom," *IEEE Trans. Signal Process.*, vol. 58, no. 8, pp. 4167-4181, 2010.
- [3] E. BouDaher, Y. Jia, F. Ahmad and M.G. Amin, "Multi-frequency co-prime arrays for high-resolution direction-of-arrival estimation," *IEEE Trans. Signal Process.*, vol. 63, no. 14, pp. 3797-3808, 2015.
- [4] K. Adhikari, J.R. Buck and K.E. Wage, "Extending coprime sensor arrays to achieve the peak side lobe height of a full uniform linear array," *EURASIP J. Adv. Signal Process.*, vol. 1, pp. 1-17, 2014.
- [5] P. Pal and P.P. Vaidyanathan, "Coprime sampling and the MUSIC algorithm," in *Proc. IEEE Digital Signal Processing Workshop and IEEE Signal Processing Education Workshop*, pp. 289-294, 2011.
- [6] K. Adhikari and J.R. Buck, "Spatial spectral estimation with product processing of a pair of colinear arrays," *IEEE Trans. Signal Process.*, under review.
- [7] S.U. Pillai, Y. Bar-Ness and F. Haber, "A new approach to array geometry for improved spatial spectrum estimation," *Proc. IEEE*, vol. 73, no. 10, pp. 1522-1524, 1985.
- [8] S.U. Pillai and F. Haber, "Statistical analysis of a high resolution spatial spectrum estimator utilizing an augmented covariance matrix," *IEEE Trans. Acoust., Speech Signal Process.*, vol. 35, no. 11, pp. 1517-1523, 1987.
- [9] V. Chavali, K.E. Wage and J.R. Buck, "Coprime processing for the Elba Island sonar data set," in *Proc. 48th Asilomar Conference on Signals, Systems and Computers*, vol. 1, pp. 1864-1868, 2014.
- [10] C.-L. Liu and P.P. Vaidyanathan, "Remarks on the spatial smoothing step in Co-array MUSIC," *IEEE Signal Process. Lett.*, vol. 22, no. 9, pp. 1438-1442, 2015.
- [11] Q. Si, Y.D. Zhang and M.G. Amin, "Generalized coprime array configurations for direction-of-arrival estimation," *IEEE Trans. Signal Process.*, vol. 63, no. 6, pp. 1377-1390, 2015.
- [12] A.B. Baggeroer and H. Cox, "Passive sonar limits upon nulling multiple moving ships with large aperture arrays," in *Proc. 33rd Asilomar Conference on Signals, Systems and Computers*, vol. 1, pp. 103-108, 1999.
- [13] H. Cox, "Adaptive beamforming in non-stationary environments," in *Proc. 36th Asilomar Conference on Signals, Systems and Computers*, vol. 1, pp. 431-438, 2002.
- [14] M.J. Hinich, "Processing spatially aliased arrays," *J. Acoust. Soc. Am.*, vol. 64, no. 3, pp. 792-794, 1978.
- [15] J.L. Moulton and S.A. Kassam, "Resolving more sources with multi-frequency coarrays in high-resolution direction-of-arrival estimation," in *Proc. 43rd IEEE Annual Conference on Information Sciences and Systems*, pp. 772-777, 2009.
- [16] Y. Liu and J.R. Buck, "Spatial Spectral Estimation Using a Coprime Sensor Array with the Min Processor," in *Proc. 9th IEEE Sensor Array and Multichannel Signal Processing*, Rio de Janeiro, Brazil, 2016.
- [17] T.-J. Shan, M. Wax and T. Kailath, "On spatial smoothing for direction-of-arrival estimation of coherent signals," *IEEE Trans. Acoust. Speech Signal Process.*, vol. 33, no. 4, pp. 806-811, 1985.